

Article

Compressive Behavior of Stainless Steel–Concrete–Carbon Steel Double-Skin Tubular (SCCDST) Members Subjected to External Hydraulic Pressure

Jian-Tao Wang ^{1,2,*}, Kai-Lin Yang ^{1,2} and Jia-Yao Sun ³

¹ School of Civil Engineering, Xi'an University of Architecture and Technology, Xi'an 710055, China

² Key Lab of Structural Engineering and Earthquake Resistance, Ministry of Education (XAUAT), Xi'an 710055, China

³ Shaanxi Province Institute of Water Resources and Electric Power Investigation and Design, Xi'an 710001, China

* Correspondence: sdwftw@163.com

Abstract: The new-type stainless steel–concrete–carbon steel double-skin tubular (SCCDST) members, characterized by their exceptional corrosion resistance and mechanical bearing capacity, have promising applications in ocean engineering, particularly in deep-water engineering. The external hydraulic pressure and interfacial action of various materials intensify the complexity of composite performance of SCCDST members. This paper describes an analytical investigation on the concentric compressive performance of SCCDST members under external hydraulic pressure. The full-range mechanism, including load–displacement response, bearing capacity contribution, and contact pressures, was investigated through the finite element (FE) model that was validated by the failure mode, bearing capacity, and response of axial load versus strain. Subsequently, influences of key geometric–physical parameters were analyzed, e.g., diameter-to-thickness ratios (D_o/t_o , D_i/t_i), material strengths (f_{yo} , f_{yi} , and f_c), hollow ratios (χ), and water depths (H). Typical results indicate that: the initial active confinement action derived from the hydraulic pressure can enhance the interfacial contact pressure and axial compression capacity of SCCDST members due to the tri-axial compression state; the enhancement of confinement effect is mainly from the interfacial interaction between outer stainless steel tube and concrete infill; influence of water depth on bearing capacity cannot be ignored, e.g., the bearing capacity of an SCCDST member with larger hollow ratio ($\chi = 0.849$) is not enhanced under a higher hydraulic pressure ($H = 900$ m) because of the cross-sectional buckling failure risk. Finally, a modified method considering the effect of water depth was proposed and verified for SCCDST members under hydraulic pressure.

Keywords: SCCDST members; stainless steel; hydraulic pressure; compressive behavior; full-range mechanism; design method



Citation: Wang, J.-T.; Yang, K.-L.; Sun, J.-Y. Compressive Behavior of Stainless Steel–Concrete–Carbon Steel Double-Skin Tubular (SCCDST) Members Subjected to External Hydraulic Pressure. *J. Mar. Sci. Eng.* **2024**, *12*, 406. <https://doi.org/10.3390/jmse12030406>

Academic Editor: José António Correia

Received: 13 January 2024

Revised: 23 February 2024

Accepted: 23 February 2024

Published: 26 February 2024



Copyright: © 2024 by the authors. Licensee MDPI, Basel, Switzerland. This article is an open access article distributed under the terms and conditions of the Creative Commons Attribution (CC BY) license (<https://creativecommons.org/licenses/by/4.0/>).

1. Introduction

Corrosion damage in ocean environments has received significant attention for steel or steel–concrete structures, such as pile foundations and jacket platforms [1,2]. As a typical high-performance structure, concrete-filled double-skin steel tubular (CFDST) structures increasingly demonstrate a promising application in ocean engineering for bearing complex loads [3–6]. Nevertheless, the traditional CFDST structure typically comprises double-skin carbon steel tubes and sandwich concrete, referred to as the concrete-filled double-skin carbon steel tubular (CFDSCST) section, which is prone to corrosion [5–7]. Consequently, a new type of double-skin composite member, i.e., stainless steel–concrete–carbon steel double-skin tubular (SCCDST) members, has been proposed to enhance the corrosion resistance of CFDSCST members (Figure 1) [8,9]. The utilization of SCCDST members is

expected to expand significantly in coastal and deep-sea engineering projects. Design methods suitable for land engineering are ever-improving for double-skin composite members with CFDCST or SCCDST sections [6–13]. In contrast to land sites, the deep-water environment subjects SCCDST members to external hydraulic pressure, where the composite performance is influenced by the combination of passive and active confinement actions (Figure 2) [13]. The passive confinement action refers to the interactive behavior between the double-skin stainless or steel tubes and sandwich concrete, and the active action is derived from the external hydraulic pressure. The design method mentioned earlier, based on passive confinement action, is no longer applicable to deep-sea engineering [14,15]. Therefore, it is vital and necessary to conduct research on the mechanical performance and calculation theory of SCCDST members under hydraulic pressure in order to provide guidance for deep-water projects.



Figure 1. Potential engineering utilization of SCCDST members for avoiding corrosion.

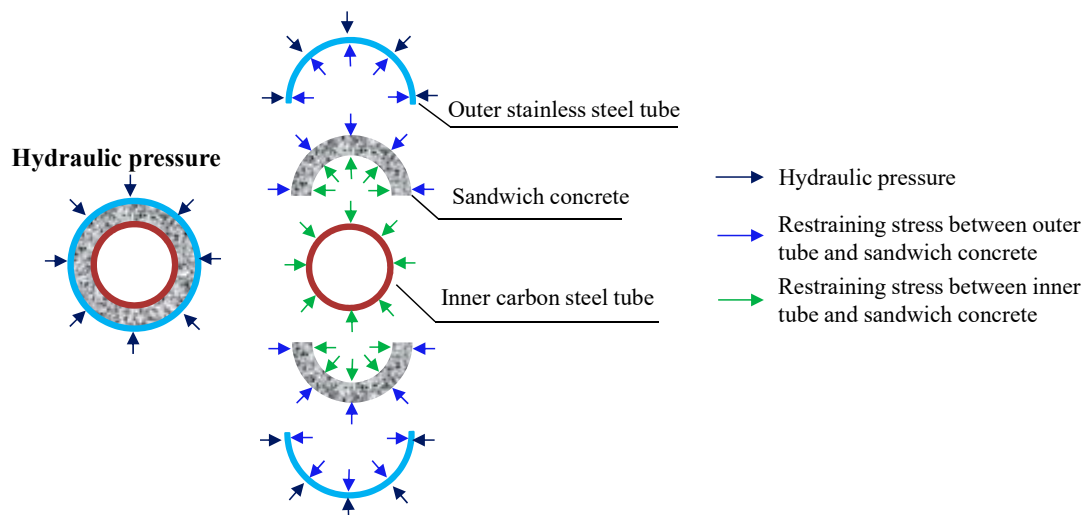


Figure 2. Confinement action under external hydraulic pressure.

The CFDCST members including the traditional CFDCST members and new-type SCCDST members are usually used as the structural members that mainly undergo axial compression. Research on the axial compressive behavior can provide a fundamental reference for their design and construction. Extensive work has been carried out on the axial compressive behavior of conventional CFDCST members [7,10,11,14,16–24]. Similarly, in order to enhance corrosion resistance, the performance of SCCDST members under concentric compression is gradually being examined [9,12,15,25–31]. It should be noted that those abovementioned studies about CFDCST and SCCDST members are mainly limited to the application scenario of land engineering with passive confinement action. For example, Li et al. [25] experimentally researched the axial compression performance

of circular-in-circular double-skin stainless steel tubular composite columns filled with seawater sea sand concrete, revealing that the cross-sectional hollow ratio has a slight impact on the concrete’s ultimate stress and member’s post-peak behavior. Wang et al. [26] investigated the mechanical property of axially compressed circular-in-circular CFDST stub members with outer stainless steel tubes through numerical and experimental methods, in which the investigation on applicability of current design codes points out that the methods in EC4 [32] and AS 5100 [33] tend to predict unsafe results and the methods in AISC 360 [34] and ACI 318 [35] can lead to a scattered and conservative prediction. Results of Castanheira et al. [29] demonstrate that SCCDST members with recycled aggregate concrete can perform a similar concentric compressive behavior compared to the SCCDST members using traditional concrete, and double-skin tubes can be easily locally buckled combined with apparently lower bearing capacity in the case of high void ratios.

Research on SCCDST members in ocean environments, especially for deep-water conditions, is still limited. Wang and Han [15] numerically analyzed the concentric compressive behavior and flexural behavior of submarine pipelines under external and inner hydraulic pressures, where the cross-section is composed of carbon steel outer pipe, sandwich concrete, and stainless steel inner pipe, and it reveals that the confinement action between double-skin pipes and sandwiched concrete is significantly affected by the hydraulic pressure. However, the influence of various external hydraulic pressures, specifically the variations in water depths, on the confinement action and composite mechanism of new-type SCCDST members remains undisclosed. The accuracy of existing design codes applicable to land engineering, such as T/CCES 7-2020 [36] and T/CECS 952-2021 [37], cannot be guaranteed when it comes to bearing capacity calculation, parameter matching, and structural measures for deep-water engineering. The application of SCCDST structures in ocean projects, such as deep-water jacket platforms and pile foundations, is hindered by a research deficiency in design methodology and mechanical mechanisms. Hence, it is essential to carry out analytical work on the aforementioned details of SCCDST members under external hydraulic pressure to address this issue.

This paper presents a numerical investigation on the analytical axial compressive behavior of SCCDST members subjected to external hydraulic pressure. A finite element (FE) model is constructed and validated based on failure mode, bearing capacity assessment, and complete load–displacement curves. The effects of key parameters (e.g., D_o/t_o , D_i/t_i , f_{y0} , f_{yi} , f_c , χ) are examined for various water depths ranging from 0 m to 900 m. Subsequently, a modified design approach is proposed to calculate the axial compressive strength for deep-water engineering applications. The findings of this study can provide valuable design references for the construction of ocean engineering projects.

2. Finite Element Modeling

2.1. Establishment of FE Model

To analyze the nonlinear behavior of inner carbon steel tubes, a constitutive relationship consisting of five stages was adopted [38,39], as shown in Figure 3, including two horizontal plastic parts. The confined concrete model under compressive loading of Han was utilized to calculate the performance of sandwich concrete [40]:

$$\frac{\sigma}{f_c} = \begin{cases} 2 \cdot \frac{\epsilon}{\epsilon_0} - \left(\frac{\epsilon}{\epsilon_0}\right)^2 & \left(\frac{\epsilon}{\epsilon_0} \leq 1\right) \\ \frac{\frac{\epsilon}{\epsilon_0}}{\beta_0 \cdot \left(\frac{\epsilon}{\epsilon_0} - 1\right)^2 + \frac{\epsilon}{\epsilon_0}} & \left(\frac{\epsilon}{\epsilon_0} > 1\right) \end{cases} \quad (1)$$

where $\frac{\epsilon}{\epsilon_0}$ is the dimensionless strain; $\frac{\sigma}{f_c}$ is the nondimensional stress. The peak strain ϵ_0 and computing coefficient β_0 are given as follows.

$$\begin{cases} \epsilon_0 = (1300 + 12.5 \cdot f_c) \times 10^{-6} + 800 \cdot \zeta^{0.2} \times 10^{-6} \\ \beta_0 = (2.36 \times 10^{-5})^{[0.25 + (\zeta - 0.5)^7]} \cdot (f_c)^{0.5} \cdot 0.5 \geq 1.12 \end{cases} \quad (2)$$

where ζ is the confinement coefficient [40]. Its tensile behavior was modeled by the fracture energy method:

$$f_{t0} = 0.26 \times (1.25f_c)^{2/3} \tag{3}$$

$$G_F = 73(f_c)^{0.18} \tag{4}$$

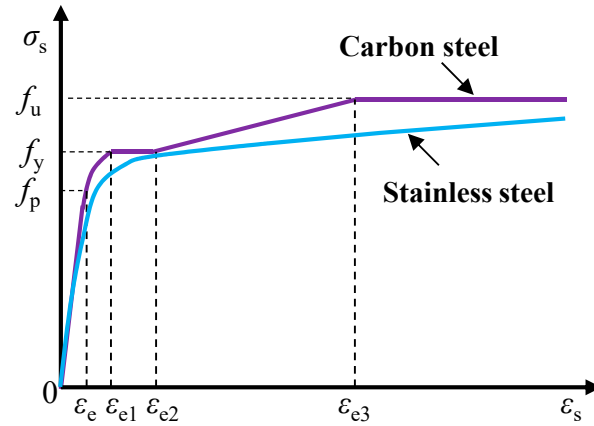


Figure 3. Constitutive relationships for carbon steel and stainless steel.

As for the stainless steel in Figure 3, it usually has a strong nonlinear stress–strain relationship; therefore, the method proposed by Rasmussen was herein adopted to simulate the outer austenitic stainless steel tube [41]:

$$\epsilon_s = \begin{cases} \frac{\sigma_s}{E_0} + 0.002 \left(\frac{\sigma_s}{\sigma_{0.2}} \right)^n & \sigma_s \leq \sigma_{0.2} \\ \frac{\sigma_s - \sigma_{0.2}}{E_{0.2}} + \epsilon_{ssu} \left(\frac{\sigma_s - \sigma_{0.2}}{\sigma_{ssu} - \sigma_{0.2}} \right)^m + \epsilon_{0.2} & \sigma_s > \sigma_{0.2} \end{cases} \tag{5}$$

$$E_{0.2} = \frac{E_0}{1 + 0.002n/e} \tag{6}$$

$$e = \frac{\sigma_{0.2}}{E_0}; n = \frac{\ln(20)}{\ln(\sigma_{0.2}/\sigma_{0.01})} \tag{7}$$

$$m = 1 + 3.5 \frac{\sigma_{0.2}}{\sigma_{ssu}} \tag{8}$$

$$\sigma_{ssu} = \sigma_{0.2} \left[\frac{1 - 0.0375(n - 5)}{0.2 + 185e} \right] \tag{9}$$

$$\epsilon_{ssu} = 1 - \frac{\sigma_{0.2}}{\sigma_{ssu}} \tag{10}$$

$$\epsilon_{0.2} = \frac{\sigma_{0.2}}{E_0} + 0.002 \tag{11}$$

The sandwich concrete and double-skin tubes (stainless steel and carbon steel) were simulated using the C3D8R solid element and S4R shell element, respectively, where the mesh sizes in the circumferential direction and longitudinal direction were equally divided into thirty-two elements and thirty elements after the sensitivity analysis of mesh size, respectively. Moreover, the mesh size through the thickness direction of sandwich concrete was set as six layers. The normal and tangential interactions of the stainless steel–concrete–carbon steel interfaces were computed using the hard contact method and Coulomb friction method. The friction coefficient was set to 0.6 [38]. No experimental investigations have been conducted on the concentric compressive behavior of SCCDST members subjected to external hydraulic pressure. Therefore, the analytical finite element (FE) model was initially validated by performing tests without hydraulic pressure (0 MPa). Subsequently, the validated FE model was further enhanced to analyze the axial compressive behavior of SCCDST members under different external hydraulic pressures. In these

aforementioned FE models, the axial load was applied using a displacement-controlled mode, where the FE models with hydraulic pressures were initially subjected to the target pressures before the application of axial load (Figure 4). Validation details and further analytical behavior are displayed in subsequent sections.

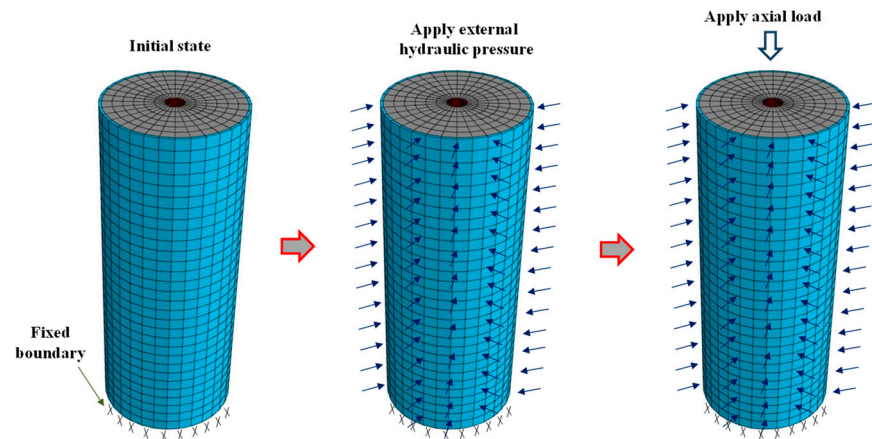


Figure 4. Established FE model.

2.2. Validation of FE Model

In order to validate the established FE model, the collected test results from a previous study [26] were compared against the failure mode, axial bearing capacity, and curve of load versus axial strain. The FE model implemented in Figure 5 demonstrates good agreement with the occurrence of local buckling in the double-skin tubes, as well as the crushing of concrete. The comparison between the anticipated axial compressive strengths (N_{FE}) and the corresponding test strengths (N_T) of SCCDST members in Table 1 demonstrates the accurate predictive capabilities of the FE model, with a mean value N_{FE}/N_T of 0.9985. In Figure 6, the typical full-range axial load versus strain curves of the tested SCCDST members are compared, considering the limitation of page space. It can be observed that the load–displacement curves of the FE models exhibit favorable agreement with the pre-peak stiffness, ultimate load-carrying capacity, and nonlinear behavior during the post-peak stage of the tested SCCDST members. Given the validation of the three aspects mentioned above, the established FE model can effectively simulate the compressive behavior of SCCDST specimens and can provide basic guidance for the analysis of axial compression performance under deep-water pressure.

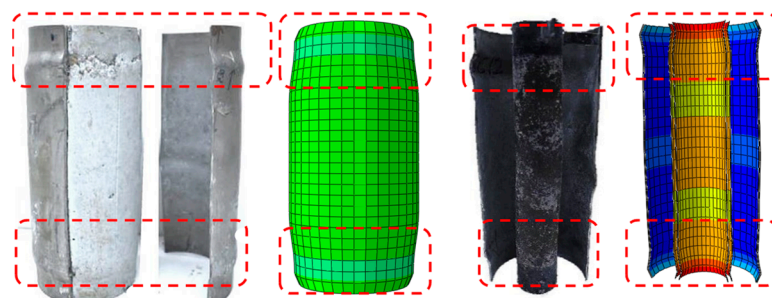


Figure 5. Verification of failure mode [26].

2.3. Analysis on Full-Range Performance with Hydraulic Pressure

Using the verified FE model, this section examines the concentric compressive performance of SCCDST members subjected to hydraulic pressure in deep-water conditions. A representative member at a water depth of 300 m is presented to enhance comprehension, and its geometric–physical characteristics are as follows: the outer stainless steel tube has a diameter of $D_o = 165$ mm and a wall thickness of $t_o = 3$ mm; the inner carbon steel tube has

a diameter of $D_i = 90$ mm and a wall thickness of $t_i = 4$ mm; steel yield strengths of outer and inner tubes are $f_{y_o} = 280$ MPa and $f_{y_i} = 960$ MPa, respectively; the concrete strength is $f_c = 80$ MPa; the length of the member is 413 mm; the water pressure at a depth of 300 m is considered to be approximately 3 MPa.

Table 1. Verification of bearing capacity.

Specimen [26]	Length/ mm	Outer Tube/mm		Inner Tube/mm		Material Strength/MPa			Test Capacity N_T /kN	Numerical Capacity N_{FE} /kN	N_{FE}/N_T
		D_o	t_o	D_i	t_i	f_{y_o}	f_{y_i}	f_c			
AC140×3-HC22×4-C40	350	140.2	2.92	22.1	4.09	300	794	40.5	1410	1392	0.9872
AC140×3-HC22×4-C80	350	140.2	2.91	22.1	4.10	300	794	79.9	1845	1846	1.0005
AC140×3-HC22×4-C120	350	140.2	2.89	22.1	4.08	300	794	115.6	2321	2316	0.9978
AC140×3-HC32×6-C40	350	140.3	2.89	32.0	5.48	300	619	40.5	1423	1476	1.0372
AC140×3-HC32×6-C80	350	140.2	2.92	31.9	5.27	300	619	79.9	2012	2020	1.0040
AC140×3-HC32×6-C120	350	140.1	2.91	31.9	5.36	300	619	115.6	2537	2566	1.0114
AC140×3-HC38×8-C40	350	140.1	2.91	38.1	7.63	300	433	40.5	1626	1633	1.0043
AC140×3-HC38×8-C80	350	140.1	2.90	38.0	7.51	300	433	79.9	2083	2072	0.9947
AC140×3-HC38×8-C120	350	140.2	2.90	37.9	7.39	300	433	115.6	2500	2483	0.9932
AC140×3-HC55×11-C40	350	140.2	2.90	55.1	10.62	300	739	40.5	2543	2539	0.9984
AC140×3-HC55×11-C80	350	140.1	2.90	55.2	10.76	300	739	79.9	2775	2877	1.0368
AC140×3-HC89×4-C40	350	140.1	2.87	89.0	3.89	300	1029	40.5	2025	2026	1.0005
AC140×3-HC89×4-C80	350	140.1	2.86	89.1	3.91	300	1029	79.9	2107	2119	1.0057
AC140×3-HC89×4-C120	350	140.2	2.88	89.1	3.91	300	1029	115.6	2195	2176	0.9913
AC165×3-HC22×4-C40	413	165.3	2.94	22.0	4.14	276	794	40.5	1750	1598	0.9131
AC165×3-HC22×4-C80	413	165.2	2.94	22.1	4.09	276	794	79.9	2413	2389	0.9901
AC165×3-HC22×4-C120	413	165.3	2.94	22.1	4.04	276	794	115.6	2911	2995	1.0289
AC165×3-HC32×6-C40	413	165.3	2.93	31.9	5.35	276	619	40.5	1943	1980	1.0190
AC165×3-HC32×6-C40R	413	165.3	2.94	31.9	5.39	276	619	40.5	1891	1825	0.9651
AC165×3-HC32×6-C80	413	165.3	2.94	31.8	5.25	276	619	79.9	2550	2540	0.9961
AC165×3-HC89×4-C40	413	165.5	2.92	89.0	3.92	276	1029	40.5	2375	2353	0.9907
AC165×3-HC89×4-C80	413	165.4	2.91	89.1	3.91	276	1029	79.9	2580	2566	0.9946
AC165×3-HC89×4-C120	413	165.2	2.92	88.9	3.88	276	1029	115.6	2671	2681	1.0037
Mean											0.9985
Variance											0.0006

Analysis on the full-range behavior of an SCCDST member with deep-water hydraulic pressure is offered in Figures 7 and 8, in which its performance response is compared to its counterpart without hydraulic pressure. Generally, the variation trend of SCCDST members with hydraulic pressure behaves analogously to that of the SCCDST member without hydraulic pressure, but the member exposed to deep-water hydraulic pressure displays a higher bearing capacity to resist axial load with an increased percentage of 10.04%, where the contributions of inner carbon steel tubes are nearly the same for both. In the condition of hydraulic pressure, the contribution of the outer stainless steel tube is slightly higher than that of the member without hydraulic pressure. The primary disparity that leads to the augmentation of load-bearing capacity can be attributed to the enhanced contribution of sandwich concrete when subjected to an elevated level of tri-axial compression in hydraulic pressure, therefore resulting in the higher axial strength or von Mises stress in Figure 9. Moreover, through the curve of axial load versus strain in Figure 7, three typical stages can be divided by four feature points for the SCCDST member with hydraulic pressure. During the stage OA, the SCCDST member is in an elastic working state. Subsequently, the outer stainless steel tube, sandwich concrete, and inner carbon steel tube gradually show elastic–plastic performance, in which the material strengths of cross-sectional materials are fully utilized. At point B, the sandwich concrete, inner tube, and outer tube contribute 57.08%, 28.45%, and 14.47% of the total axial bearing capacity of the SCCDST member, respectively. During the stage O-A-B, the confining stress between the outer stainless steel tube and sandwich concrete is increased quickly (Figure 8a), but

the confining stress of the inner carbon steel tube and concrete gradually degrades to zero, as displayed in Figure 8b. Thereafter, the SCCDST member progresses to the failure phase accompanied by capacity degradation, while the concrete undergoes severe crushing and the outer or inner tubes reach a highly plastic state, resulting in the rapid increase in confining stress of the outer tube to concrete (Figure 8a). As illustrated in Figure 8, the existing hydraulic pressure promotes the composite performance between double-skin tubes and concrete infill, leading to an initial active confining stress and a heightened state of the full-range process, from which the confining stress between the inner tube and sandwich concrete is comparatively lower than that between the outer tube and concrete, and it rapidly decreases before reaching the maximum load point B.

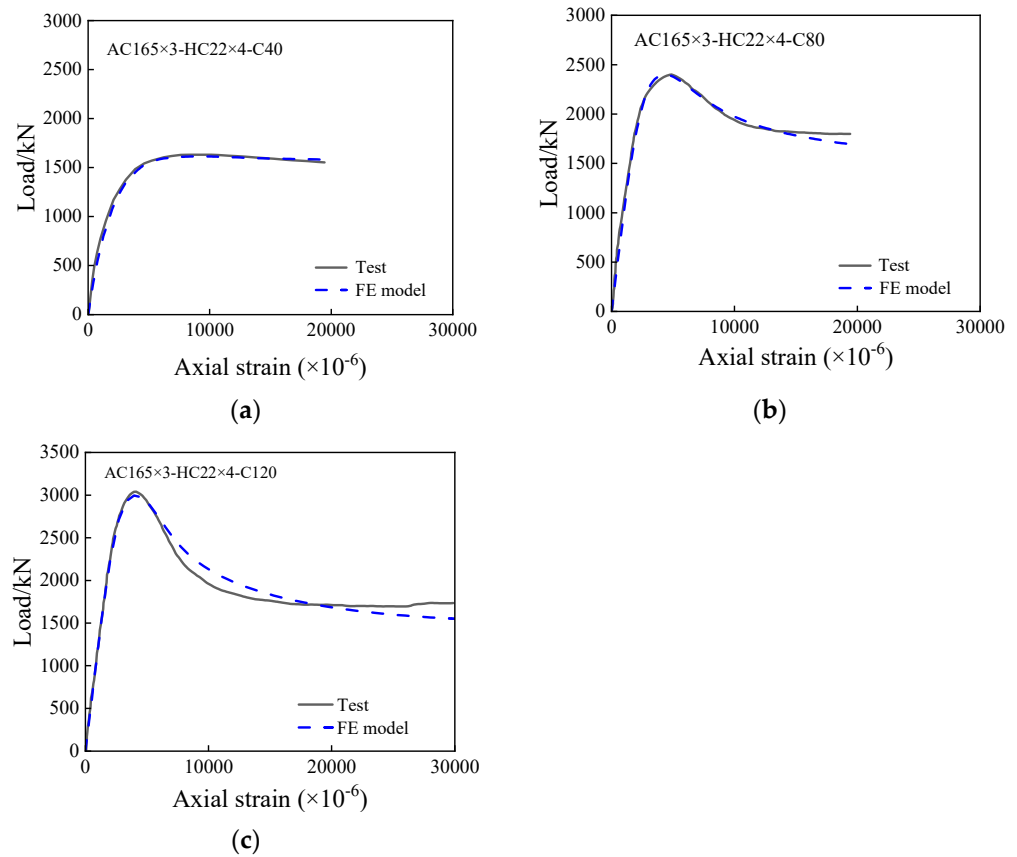


Figure 6. Verification of load–displacement curves. (a) AC165×3-HC22×4-C40; (b) AC165×3-HC22×4-C80; (c) AC165×3-HC22×4-C120.

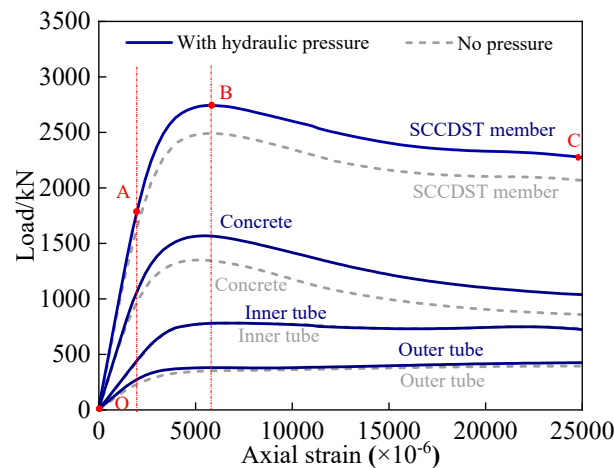


Figure 7. Analysis on full-range axial load–strain curves.

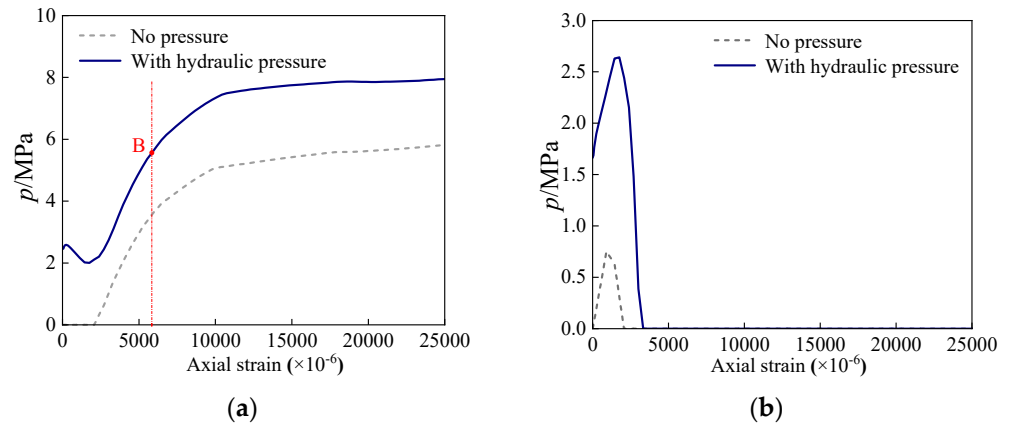


Figure 8. Analysis on confinement effect. (a) Confining stress between outer stainless steel tube and sandwich concrete; (b) Confining stress between inner carbon steel tube and sandwich concrete.

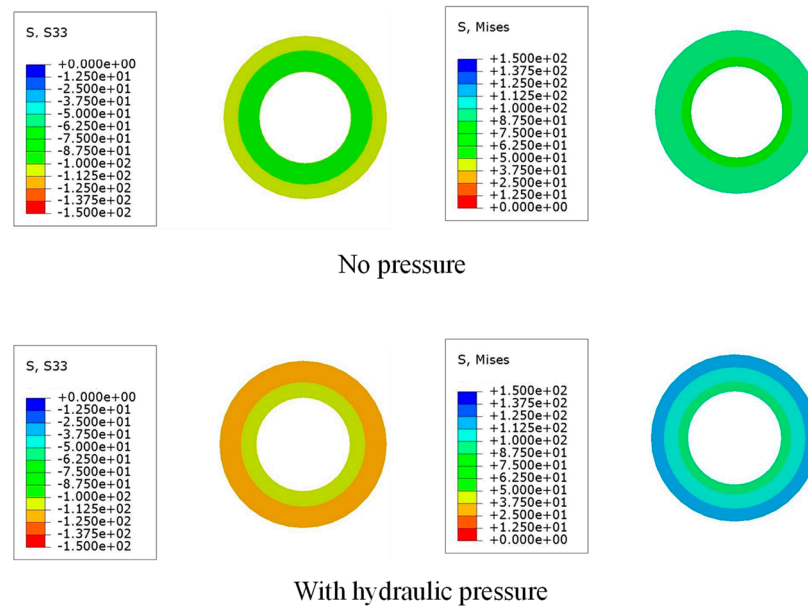


Figure 9. Stress-field nephogram of sandwich concrete at peak load.

3. Parametric Study

This section displays the result of a parametric study, including the influences of diameter-to-thickness ratio of outer stainless steel tube (D_o/t_o), diameter-to-thickness ratio of inner carbon steel tube (D_i/t_i), material strengths (f_{y0}, f_{yi} , and f_c), hollow ratio (χ), and water depth (H). A summary of the studied parameters is given in Table 2. The benchmark specimen corresponds to the member described in Section 2.3.

Table 2. Summary of studied parameters.

Water Depths (H)/m	D_o/t_o	D_i/t_i	f_{y0}/MPa	f_{yi}/Mpa	f_c/Mpa	χ
0; 300; 600; 900	110; 55; 36.7; 27.5	45; 22.5; 15; 11.25	280; 350; 420; 480	460; 550; 690; 960	40; 60; 80; 100	0.283; 0.566; 0.849

Note: χ can be calculated by the equation of $\chi = D_i/(D_o - 2t_o)$.

3.1. Influence of D_o/t_o Ratio

Influences of the D_o/t_o ratio on full-range responses are shown in Figure 10. Due to similar patterns, the analysis results at a depth of 300 m are used as an example for explanation. Altering values of D_o/t_o ratios was achieved by keeping diameter D_o consistent

but changing values of thickness t_o . The axial bearing capacity is enhanced with a decrease in the D_o/t_o ratios, while the post-peak behavior, such as ductility, is also improved (Figure 10a). When it comes to the impact on the contact pressure between double-skin tubes and sandwich concrete, reducing the D_o/t_o ratios, i.e., increasing the area of the stainless steel tube, gradually enhances the confining stress of the outer stainless steel tube on the sandwich concrete due to the improvement in the confinement coefficient, but it has an opposite impact on the confining stress of the inner tube to sand concrete because of the amplified nonuniform confinement effect. Generally, amplifying the D_o/t_o ratios causes a gradual decrease in axial bearing capacity at the same water depth (Figure 11), e.g., at the water depth $H = 300$ m, improving the D_o/t_o ratio from 27.5 to 36.7, 55, and 110, respectively, reduces the axial compressive strength by 5.16%, 11.08%, and 17.57%. And at the same value of D_o/t_o ratio, a greater water depth, namely due to higher hydraulic pressure, can enhance the axial bearing capacity for SCCDST members, e.g., for a member with $D_o/t_o = 55$, its axial compression strength is gradually increased by 7.18%, 14.51%, and 21.62% with increasing water depth from 0 m to 300 m, 600 m, and 900 m, respectively.

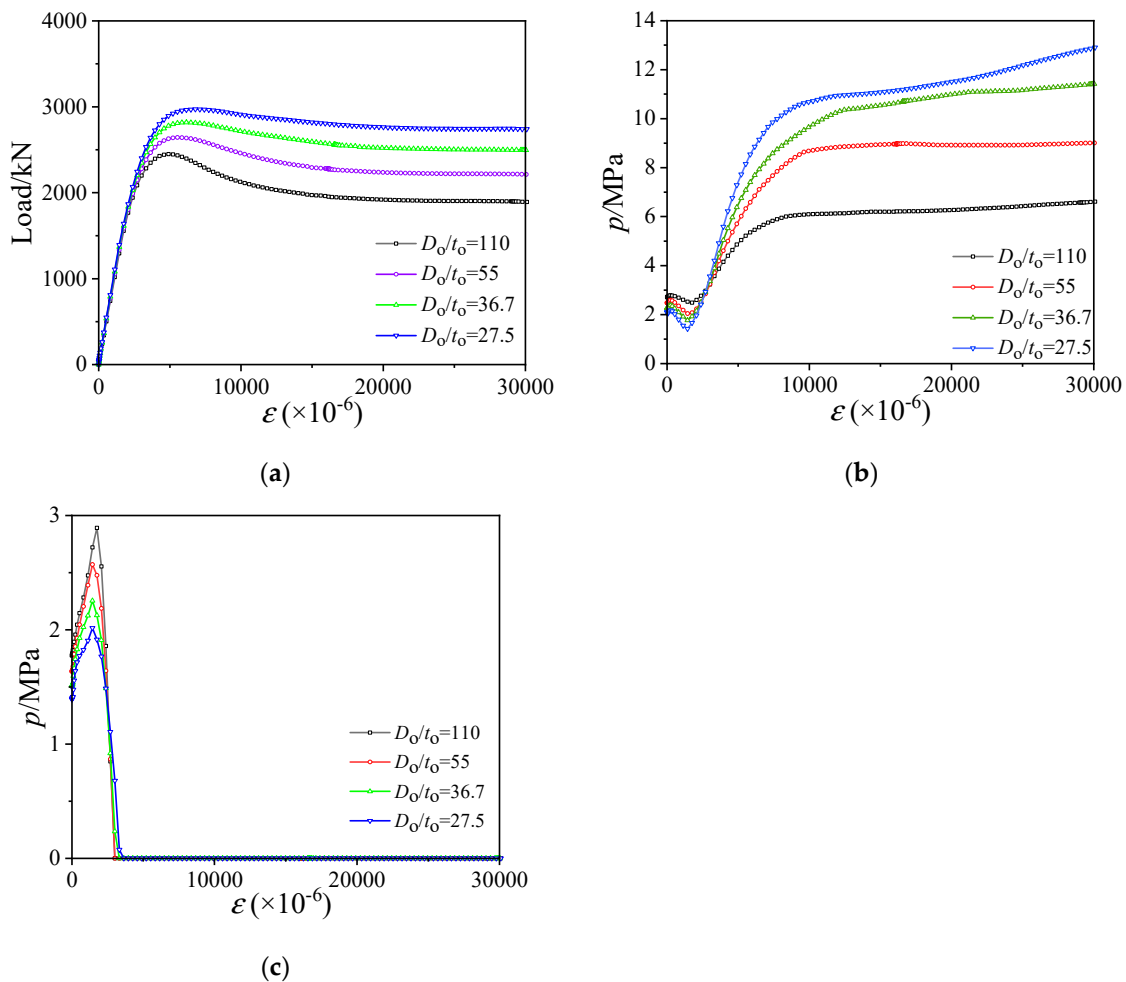


Figure 10. Influence of D_o/t_o at the water depth of 300 m. (a) Load–displacement curves; (b) Confining stress between outer stainless steel tube and sandwich concrete; (c) Confining stress between inner carbon steel tube and sandwich concrete.

3.2. Influence of D_i/t_i Ratio

Influences of D_i/t_i ratio are offered in Figures 12 and 13. Modifying the D_i/t_i ratios was accomplished by keeping the initial diameter D_i consistent while altering the values of thickness t_i . In Figure 12, increasing the D_i/t_i ratios causes a gradual decrease in the axial bearing capacity, but the D_i/t_i ratios do not significantly affect the confinement

coefficient for restricting the lateral deformation of sandwich concrete. This minor influence is observed in the confining stress between the outer stainless steel tube and sandwich concrete (Figure 12b). On the contrary, a reduced D_i/t_i ratio, indicating an increased wall thickness, enhances the local buckling resistance of the inner tube, thereby reinforcing the confinement effect and contact pressure in limiting concrete expansion (Figure 12c). The changing trend in the influence of the D_i/t_i ratio on bearing capacity, as depicted in Figure 13, is similar to that of the D_o/t_o ratio. For example, at the water depth $H = 300$ m, enhancing the D_i/t_i ratio from 11.25 to 15, 22.5, and 45, respectively, decreases the axial bearing capacity by 10.62%, 21.49%, and 33.41%; at $D_i/t_i = 15$, increasing water depth from 0 m to 300 m, 600 m, and 900 m gradually enhances the bearing capacity by 3.89%, 10.11%, and 16.17%, respectively.

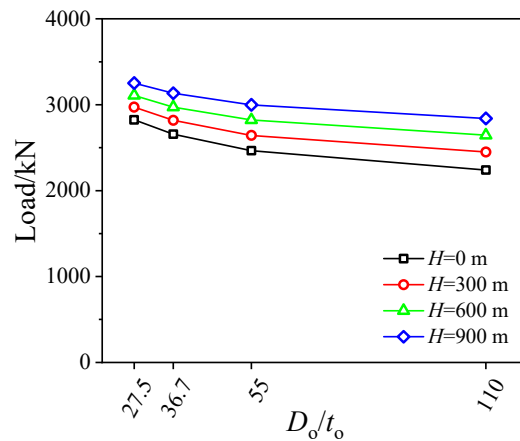


Figure 11. Influence of D_o/t_o on bearing capacity at various water depths.

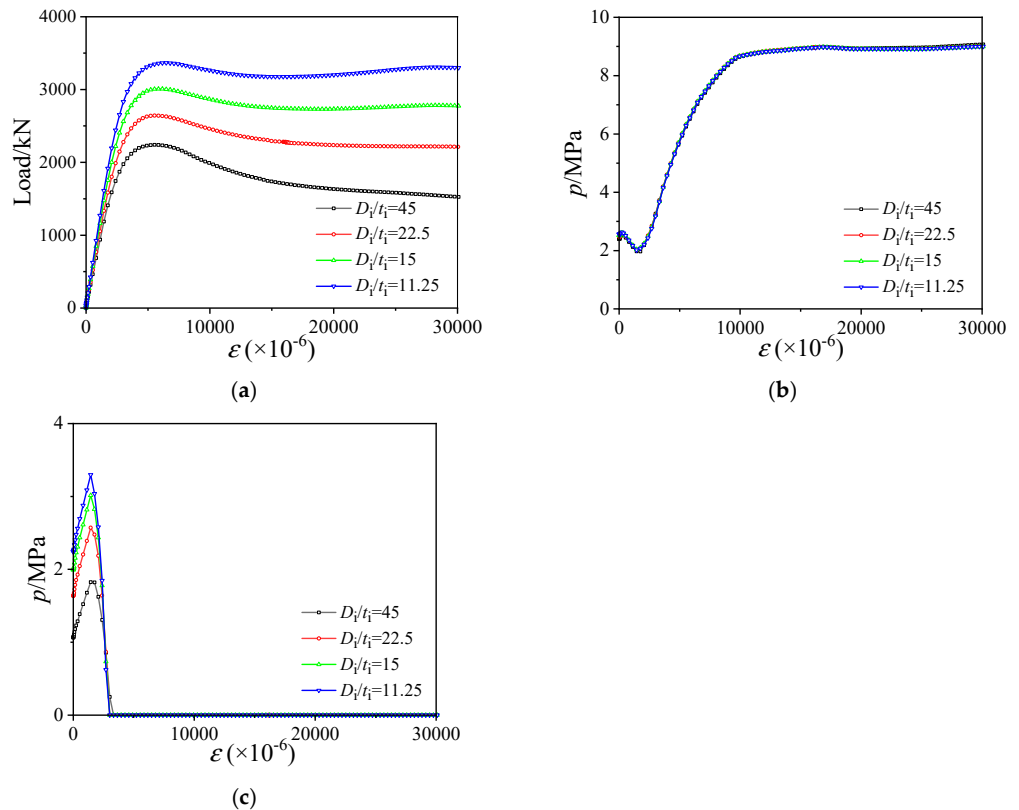


Figure 12. Influence of D_i/t_i at the water depth of 300 m. (a) Load–displacement curves; (b) Confining stress between outer stainless steel tube and sandwich concrete; (c) Confining stress between inner carbon steel tube and sandwich concrete.

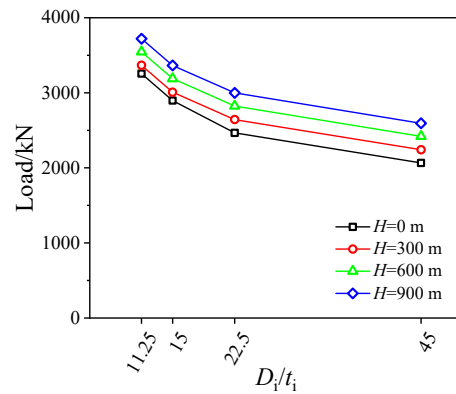


Figure 13. Influence of D_i/t_i on bearing capacity at various water depths.

3.3. Influence of f_{y0}

Influences of f_{y0} are displayed in Figures 14 and 15. Improving the yield strength of the outer stainless steel tube can directly increase the axial bearing capacity in a linear way, as shown in Figures 14a and 15, where the capacity is respectively increased by 4.61%, 8.35%, and 11.71% by enhancing yield strength f_{y0} from 280 MPa to 350 MPa, 420 MPa, and 480 MPa at the water depth of 300 m. Moreover, increasing water depth also improves the axial compression strength of SCCDST members at a certain strength of f_{y0} , e.g., at $f_{y0} = 350$ MPa, changing water depth from 0 m to 300 m, 600 m, and 900 m, respectively, enhances the bearing capacity by 6.64%, 13.53%, and 20.21%. Increasing yield strength f_{y0} actually increases the confinement coefficient, thereby enhancing the confinement stress between the outer stainless steel tube and sandwich concrete (Figure 14b), but this has a minor impact on that between the inner tube and sandwich concrete (Figure 14c).

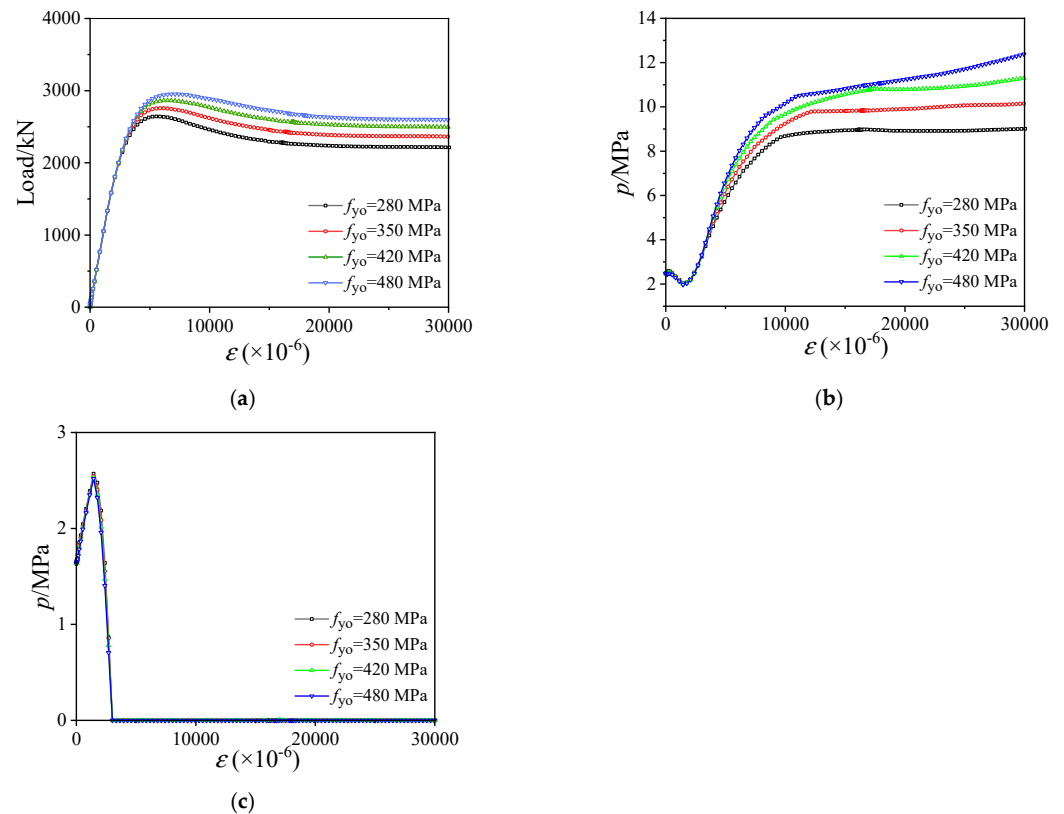


Figure 14. Influence of f_{y0} at the water depth of 300 m. (a) Load–displacement curves; (b) Confining stress between outer stainless steel tube and sandwich concrete; (c) Confining stress between inner carbon steel tube and sandwich concrete.

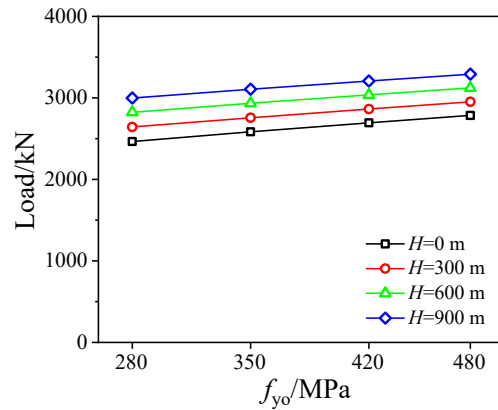


Figure 15. Influence of f_{yo} on bearing capacity at various water depths.

3.4. Influence of f_{yi}

Influences of f_{yi} are illustrated in Figures 16 and 17. Similar to the effect of yield strength f_{yo} , increasing yield strength f_{yi} also has a positively correlated growth effect on axial compression strength. For example, the axial bearing capacity is respectively enhanced by 3.58%, 9.00%, and 18.82% when improving f_{yi} from 460 MPa to 550 MPa, 690 MPa, and 960 MPa at the water depth of 300 m; at $f_{yi} = 690$ MPa, increasing water depth from 0 m to 300 m, 600 m, and 900 m, respectively, improves the axial compression capacity by 7.73%, 15.63%, and 23.29%. As for the confining stress between the double-skin tubes and sandwich concrete in Figure 16b,c, altering yield strength f_{yi} has a slight impact on it, revealing that the inner tube mainly contributes to axial compression strength by working as an independent part.

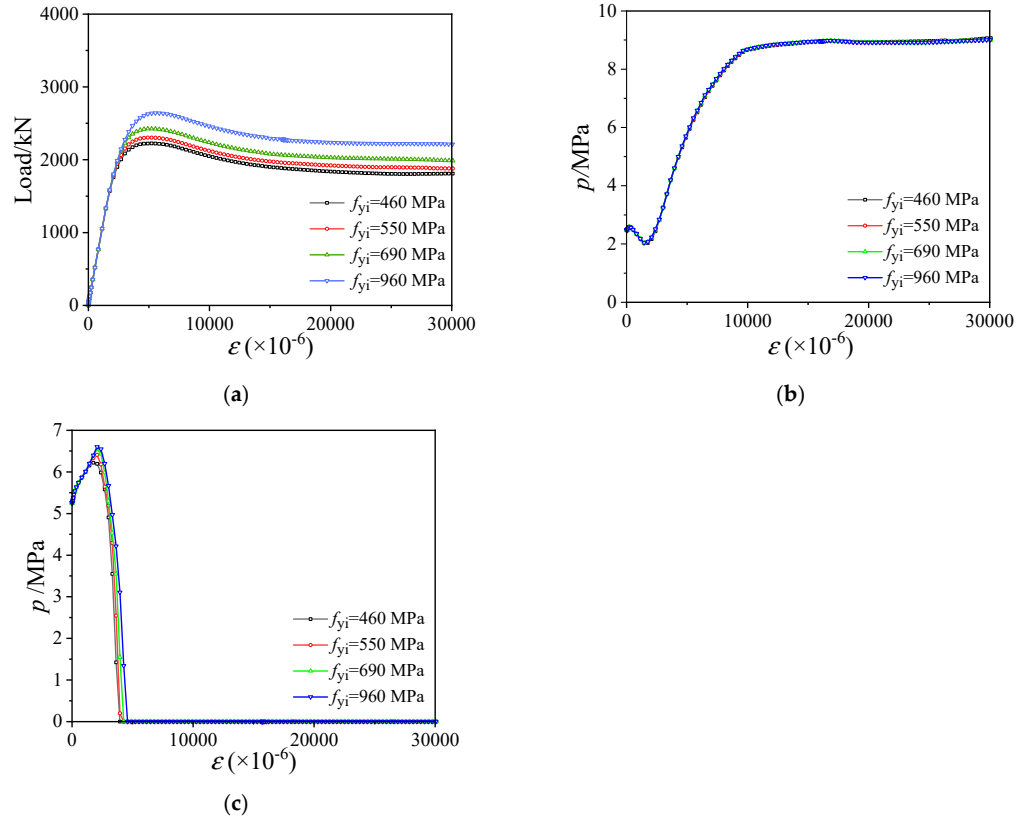


Figure 16. Influence of f_{yi} at the water depth of 300 m. (a) Load–displacement curves; (b) Confining stress between outer stainless steel tube and sandwich concrete; (c) Confining stress between inner carbon steel tube and sandwich concrete.

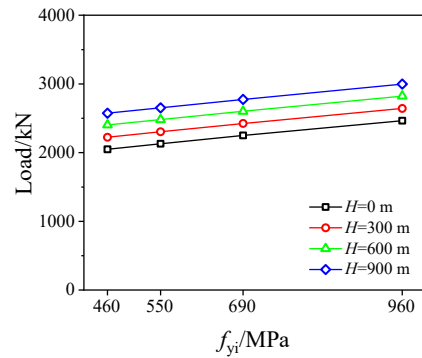


Figure 17. Influence of f_{yi} on bearing capacity at various water depths.

3.5. Influence of f_c

Figures 18 and 19 display the influences of concrete strength f_c . As shown in Figure 18a, increasing the strength of f_c greatly improves the axial compression capacity of SCCDST members. However, it also accelerates the degradation trend of the post-peak stage due to the brittleness of high-strength concrete. Regarding the effect on confining stress in Figure 18b, enhancing the concrete strength f_c can slightly reduce interfacial interaction during the pre-peak stage (axial strain < 5000 $\mu\epsilon$) owing to the decreased confinement coefficient; thereafter, the evolution trend is reversed, because the higher the strength of the concrete, the more prone it is to brittle failure, resulting in increased lateral deformation and increased contact pressure on the steel tube. The change in confining stress of the inner steel tube to sandwich concrete is also the same (Figure 18c). Increasing f_c causes a linear increase in bearing capacity, as depicted in Figure 19, e.g., enhancing f_c from 40 MPa to 60 MPa, 80 MPa, and 100 MPa at the water depth of 300 m respectively increases the axial compression strength by 11.68%, 23.70%, and 36.21%. On the other hand, the axial bearing capacity is respectively improved by 6.75%, 13.53%, and 20.11% while gradually deepening water depth from 0 m to 900 m at the condition of $f_c = 100$ MPa. Influence of water depth (i.e., the hydraulic pressure) on the load-carrying capacity is significant and should be taken into consideration.

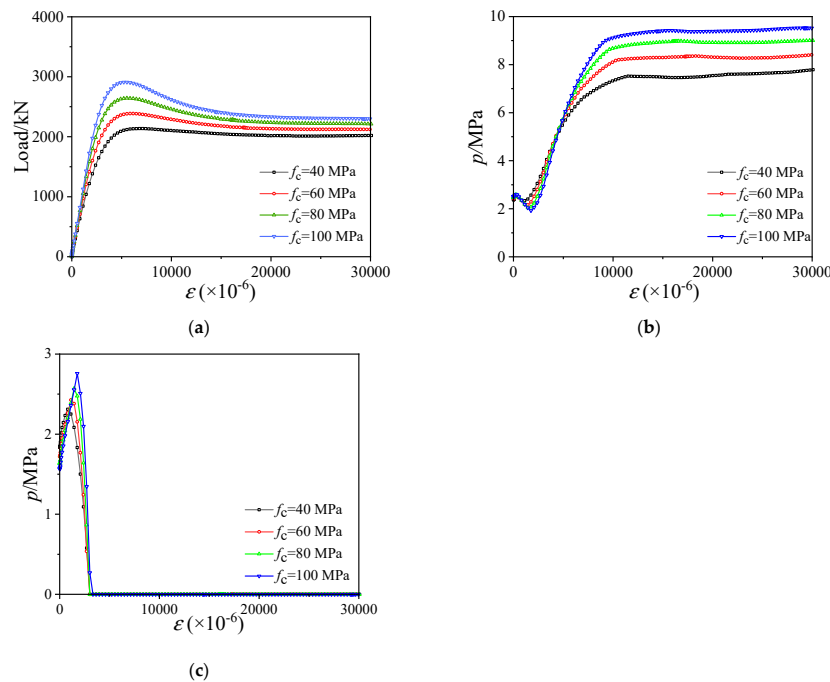


Figure 18. Influence of f_c at the water depth of 300 m. (a) Load–displacement curves; (b) Confining stress between outer stainless steel tube and sandwich concrete; (c) Confining stress between inner carbon steel tube and sandwich concrete.

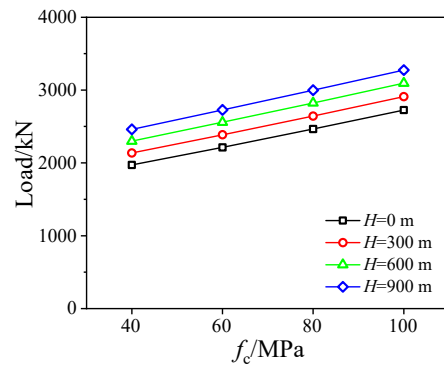


Figure 19. Influence of f_c on bearing capacity at various water depths.

3.6. Influence of χ

Influences of hollow ratio χ are displayed in Figures 20 and 21, where altering the hollow ratio is conducted by changing the diameter of the inner tube while keeping the diameter of the outer tube consistent. The results in Figure 20b,c indicate that a higher hollow ratio (e.g., $\chi = 0.849$) obviously reduces the composite behavior between double-skin tubes and sandwich concrete due to the decreased cross-sectional stiffness, thereby resulting in a decline of bearing capacity (Figure 20a), e.g., the capacity is reduced by 4.06% and 21.75% when increasing the hollow ratio from 0.283 to 0.566 and 0.849 in the case of water depth of 300 m. Moreover, regarding the influence of water depth, a marginal variation exists in the case of the greater water depth (e.g., $H = 900$ m) for the SCCDST members with larger hollow ratios (e.g., $\chi = 0.849$), reflecting that necessary measures should be conducted to control the hollow ratio in the deep-water environment where the maximum allowable hollow ratio should be stricter than that of land engineering.

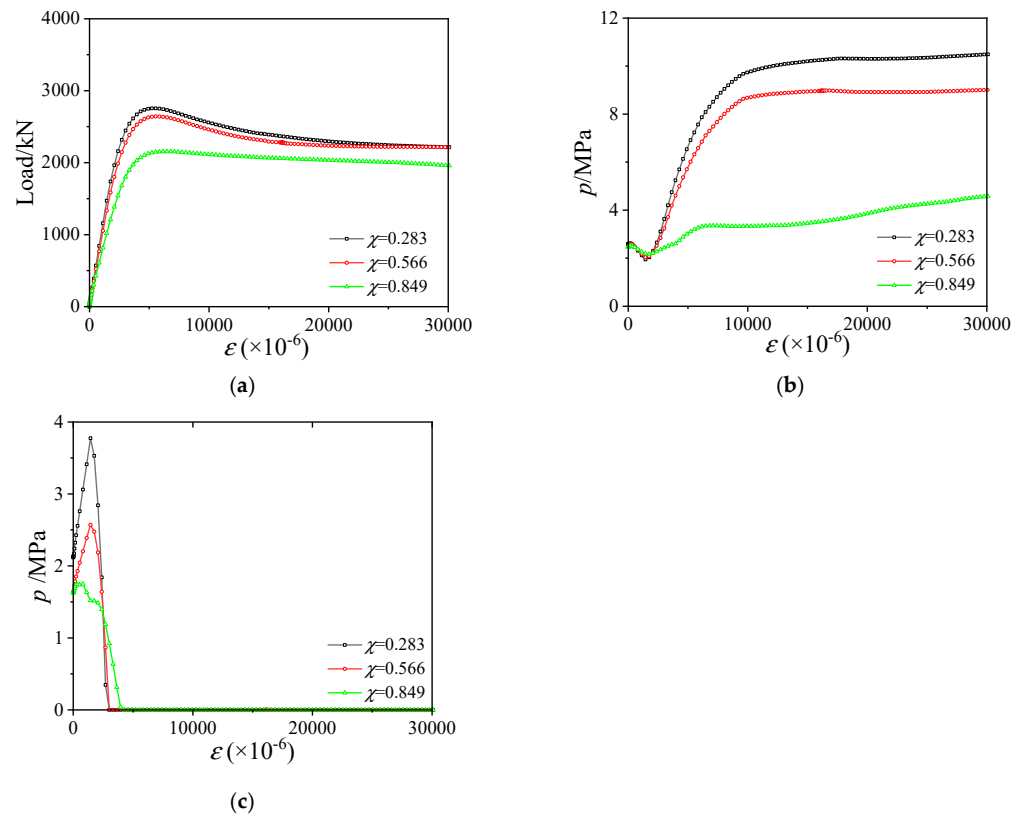


Figure 20. Influence of χ at the water depth of 300 m. (a) Load–displacement curves; (b) Confining stress between outer stainless steel tube and sandwich concrete; (c) Confining stress between inner carbon steel tube and sandwich concrete.

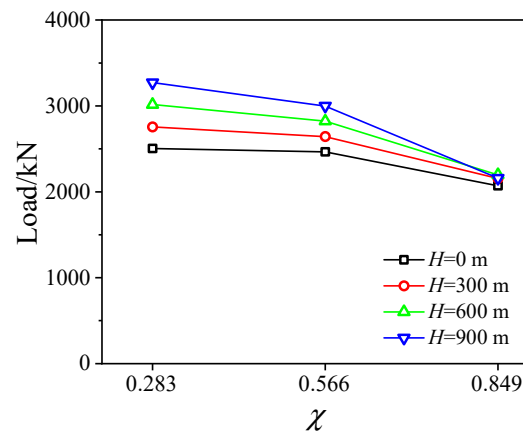


Figure 21. Influence of χ on bearing capacity at various water depths.

4. Design Method on Bearing Capacity

In the current design system, the typical design codes, e.g., T/CCES 7-2020 [36] and T/CECS 952-2021 [37], mainly focus on land engineering using traditional CFDST members with carbon steel tubes and solid concrete-filled stainless steel tubular members, therefore, no available design method is suitable for new-type SCCDST members, especially for the deep-water service environment. In this section, a modified method for SCCDST members is proposed based on the existing design method. Details of the modification procedures are as follows.

In the design code T/CCES 7-2020 [36], the axial compression capacity of traditional CFDST members using carbon steel can be divided into two parts, i.e., the inner tube and the composite part of sandwich concrete and the outer tube:

$$N_{CFDST} = N_{osc} + N_i \tag{12}$$

where N_{CFDST} is the axial compression capacity for the whole traditional CFDST member; N_{osc} denotes the contribution of the outer tube and sandwich concrete; N_i represents the contribution of the inner tube. By conducting a mechanism analysis and parametric study, it has been observed that the interfacial pressure between the inner tube and sandwich concrete generally leads to a subtle composite action on the SCCDST members. Therefore, for the new type, the calculation hypothesis in Equation (12) is still adopted for SCCDST members, where the contribution of the inner tube can be calculated by the following equation:

$$N_i = f_{yi}A_{si} \tag{13}$$

The capacity contribution N_{osc} can be derived from the composite strength method:

$$N_{osc} = f_{osc}(A_{so} + A_c) \tag{14}$$

Regarding the composite strength f_{osc} , there is no available equation to determine its accurate value in the case of the stainless steel tube–sandwich concrete composite part under the hollow section, in which the sandwich concrete suffers from nonuniform confining stress. The design code T/CECS 952-2021 [37] offers an equation for solid concrete-filled stainless steel tubular members, and the composite strength (f_{sc}) for the outer stainless steel tube and solid core concrete is given as:

$$\begin{cases} f_{sc} = (1.14 + 1.02\tilde{\xi})f_{ck} \\ \tilde{\xi} = \frac{A_{so} \cdot f_{yo}}{A_{cc} \cdot f_{ck}} \end{cases} \tag{15}$$

In this paper, the composite strength f_{osc} can be approximately equal to f_{sc} because the confinement effect is mainly induced by the restraint of the outer stainless tube:

$$f_{osc} = f_{sc} \tag{16}$$

In Equations (15) and (16), the prismatic compressive strength f_{ck} can be derived from the following method [42]:

$$f_{ck} = 0.4f_{cu}^{7/6} \tag{17}$$

$$f_{cu} = \begin{cases} f_c/0.8 & f_c \leq 32\text{MPa} \\ f_c + 8 & f_c > 32\text{MPa} \end{cases} \tag{18}$$

Based on the calculated results (N_{FE}) of the FE model, a verification and comparison study on SCCDST members with external hydraulic pressure was conducted to validate the applicability of the aforementioned method for composite strength f_{osc} and axial bearing capacity N_{CFDST} . The validation results are shown in Figure 22, from which it can be observed that the accuracy of the existing design method predicts a gradual decline trend with increasing water depth, reflecting that the current design methods based on terrestrial engineering specifications have become difficult to apply in evaluating the safety of deep-sea engineering bearing capacity. Hence, to evaluate the axial compression capacity of SCCDST members under deep-water hydraulic pressure, a modified method was established by nonlinear regression analysis for reflecting the influence of various depths (i.e., pressures):

$$N_{SM} = [1 - 0.00024 \cdot (300 - H)] \cdot N_{osc} \tag{19}$$

where N_{SM} is the modified load-carrying capacity for SCCDST members with hydraulic pressures. To further verify the accuracy of the modified method in Equation (19), it was also compared to the finite element results, as shown in Figure 23. Results indicate that the modified method predicts well with the capacities of SCCDST members under hydraulic pressures by obtaining an average value (N_{SM}/N_{FE}) of 0.9954. Considering the current lack of research on the SCCDST structure in deep-water environments, the above modified method can be used as a preliminary reference for engineering design and safety evaluation.

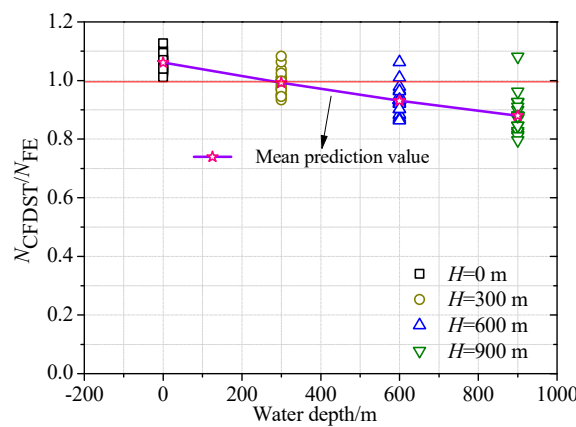


Figure 22. Prediction results of current method.

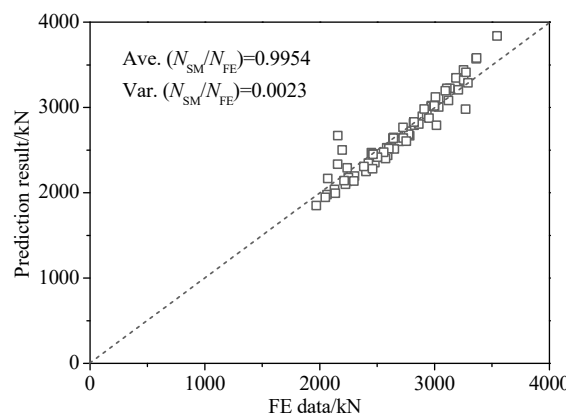


Figure 23. Verification of the modified method.

5. Conclusions

This paper demonstrates the analytical compressive behavior and design method for stainless steel–concrete–carbon steel double-skin tubular (SCCDST) members under hydraulic pressures. It can be concluded through the current research that:

(1) The developed FE models for SCCDST members are verified by the failure mode, axial bearing capacity, and curve of load versus axial strain. A reasonable agreement is well achieved.

(2) The full-range mechanism incorporating the compressive load–strain response, composite actions, and bearing capacity contribution is analyzed for SCCDST members exposed to external hydraulic pressure. The result indicates that the external hydraulic pressure subjects the SCCDST member to an elevated level of tri-axial compression, therefore resulting in the enhancement of composite action and load-bearing capacity.

(3) Influences of key parameters are examined, including the influences of D_o/t_o ratio, D_i/t_i ratio, material strengths (f_{yo} , f_{yi} , and f_c), hollow ratio (χ), and water depth (H). The geometric–physical parameters of the inner tube (e.g., D_i/t_i and f_{yi}) mainly contribute to axial compression capacity by working as an independent part due to the slight impact the interfacial contact pressure. The increased hydraulic pressure can increase the failure risk for SCCDST members with large hollow ratios (e.g., in the case of $H = 900$ m and $\chi = 0.849$), therefore the maximum allowable hollow ratio in the deep-water environment should be stricter than that of land engineering.

(4) Accuracy of the existing method in design code predicts a gradual decline tendency with increasing water depth. A modified method incorporating the influence of water depth is proposed and verified for SCCDST members under hydraulic pressure, which can be accepted as a preliminary reference for safety evaluation of deep-water engineering.

Author Contributions: Conceptualization, J.-T.W.; methodology, J.-T.W. and K.-L.Y.; validation, J.-T.W., K.-L.Y. and J.-Y.S.; formal analysis, J.-T.W. and K.-L.Y.; investigation, J.-T.W., K.-L.Y. and J.-Y.S.; resources, J.-T.W.; writing—original draft preparation, J.-T.W., K.-L.Y. and J.-Y.S.; writing—review and editing, J.-T.W. and K.-L.Y.; visualization, J.-T.W. and K.-L.Y.; supervision, J.-T.W.; project administration, J.-T.W.; funding acquisition, J.-T.W. All authors have read and agreed to the published version of the manuscript.

Funding: This research was funded by High-level Talent Research Startup Fund (No. 1608722024) of Xi'an University of Architecture and Technology.

Institutional Review Board Statement: Not applicable.

Informed Consent Statement: Not applicable.

Data Availability Statement: The data presented in this study are available on request from the corresponding author.

Acknowledgments: The authors acknowledge the numerical assistance from the team members of Xi'an Jiaotong University and Xi'an University of Architecture and Technology.

Conflicts of Interest: The authors declare no conflicts of interest.

Nomenclatures

f_c	compression strength of concrete cylinder
f_{ck}	prismatic compressive strength of concrete
f_{t0}	tensile strength of concrete
f_{yo}	yielding strength of outer steel tube
f_{yi}	yielding strength of inner steel tube
t_i or t_o	inner/outer tube's thickness
f_{osc}	composite strength of stainless steel tube–sandwich concrete composite part under the double-skin hollow section
f_{sc}	composite strength of outer tube and core concrete under solid section
f_{cu}	cubic concrete strength under compression

A_c	cross-sectional area of sandwich concrete
A_{si}	cross-sectional area of inner steel tube
A_{so}	cross-sectional area of outer steel tube
A_{cc}	area of core concrete in solid section
D_o	diameter of outer steel tube
D_i	diameter of inner steel tube
E_0	elasticity modulus
G_F	fracture energy
H	water depth
N_{CFDST}	axial compression capacity for whole traditional CFDST members
N_{osc}	axial strength contribution of outer tube and sandwich concrete
N_i	axial strength contribution of inner tube
N_{SM}	the modified load-carrying capacity for SCCDST members with hydraulic pressures
ξ	confinement coefficient
ϵ_0	peak strain
β_0	computing coefficient
ϵ_s	strain of stainless steel
σ_s	corresponding stress at strain ϵ_s
$\sigma_{0.2}$	0.2% proof stress for stainless steel
$\epsilon_{0.2}$	strain at $\sigma_{0.2}$ for stainless steel
ϵ_{ssu}	ultimate strain for stainless steel
σ_{ssu}	tensile strength for stainless steel
n and m	calculation factors
$\sigma_{0.01}$	0.01% proof stress for stainless steel
χ	hollow ratio

References

1. Qian, R.; Li, Q.; Fu, C.; Zhang, Y.; Wang, Y.; Jin, X. Atmospheric chloride-induced corrosion of steel-reinforced concrete beam exposed to real marine-environment for 7 years. *Ocean Eng.* **2023**, *286*, 115675. [\[CrossRef\]](#)
2. Xiao, L.; Peng, J.; Cai, C.S.; Chen, H. Experimental and numerical investigations on the mechanical behavior of coastal high performance steel beams with local corrosion within the shear-span. *Appl. Ocean Res.* **2023**, *136*, 103581. [\[CrossRef\]](#)
3. Peng, W.; Duan, T.; Hou, J.; Guo, W.; Ding, K.; Cheng, W.; Xu, L. Long-term corrosion behaviour of 1060 aluminium in deep-sea environment of South China Sea. *Corros. Eng. Sci. Technol.* **2021**, *56*, 327–340. [\[CrossRef\]](#)
4. Katsoudas, A.S.; Sillionis, N.E.; Anyfantis, K.N. Structural health monitoring for corrosion induced thickness loss in marine plates subjected to random loads. *Ocean Eng.* **2023**, *273*, 114037. [\[CrossRef\]](#)
5. Li, G.; Hou, C.; Shen, L. Combined compression-bending performance and design of CFST with localised pitting corrosion. *J. Constr. Steel Res.* **2022**, *192*, 107247. [\[CrossRef\]](#)
6. Li, W.; Han, L.H.; Zhao, X.L. Behavior of CFDST stub columns under preload, sustained load and chloride corrosion. *J. Constr. Steel Res.* **2015**, *107*, 12–23. [\[CrossRef\]](#)
7. Fang, Y.; Wang, Y.; Hou, C.; Lu, B. CFDST stub columns with galvanized corrugated steel tubes: Concept and axial behaviour. *Thin-Walled Struct.* **2020**, *157*, 107116. [\[CrossRef\]](#)
8. Zhao, H.; Wang, R.; Lam, D.; Hou, C.C.; Zhang, R. Behaviours of circular CFDST with stainless steel external tube: Slender columns and beams. *Thin-Walled Struct.* **2021**, *158*, 107172. [\[CrossRef\]](#)
9. Han, L.H.; Ren, Q.X.; Li, W. Tests on stub stainless steel–concrete–carbon steel double-skin tubular (DST) columns. *J. Constr. Steel Res.* **2011**, *67*, 437–452. [\[CrossRef\]](#)
10. Li, W.; Han, L.H.; Zhao, X.L. Axial strength of concrete-filled double skin steel tubular (CFDST) columns with preload on steel tubes. *Thin-Walled Struct.* **2012**, *56*, 9–20. [\[CrossRef\]](#)
11. Vernardos, S.; Gantes, C. Experimental behavior of concrete-filled double-skin steel tubular (CFDST) stub members under axial compression: A comparative review. *Structures* **2019**, *22*, 383–404. [\[CrossRef\]](#)
12. Wang, F.; Young, B.; Gardner, L. CFDST sections with square stainless steel outer tubes under axial compression: Experimental investigation, numerical modelling and design. *Eng. Struct.* **2020**, *207*, 110189. [\[CrossRef\]](#)
13. Aghamaleki, S.T.N.; Naghipour, M.; Amiri, J.V.; Nematzadeh, M. Compression behavior of the concrete-filled double skin steel tube columns under hydrostatic pressure: Experimental and modeling study. *Structures* **2023**, *58*, 105505. [\[CrossRef\]](#)
14. Cheng, Z.; Wang, F.; Zhang, D. Analytical model for axially compressed circular concrete-filled double skin steel tubes (CFDSTs): Insights from concrete non-uniformly confined states. *Thin-Walled Struct.* **2023**, *192*, 111106. [\[CrossRef\]](#)
15. Wang, F.C.; Han, L.H. Analytical behavior of carbon steel–concrete–stainless steel double-skin tube (DST) used in submarine pipeline structure. *Mar. Struct.* **2019**, *63*, 99–116. [\[CrossRef\]](#)
16. Zhao, X.L.; Tong, L.W.; Wang, X.Y. CFDST stub columns subjected to large deformation axial loading. *Eng. Struct.* **2010**, *32*, 692–703. [\[CrossRef\]](#)

17. Pagoulatou, M.; Sheehan, T.; Dai, X.H.; Lam, D. Finite element analysis on the capacity of circular concrete-filled double-skin steel tubular (CFDST) stub columns. *Eng. Struct.* **2014**, *72*, 102–112. [[CrossRef](#)]
18. Ekmekyapar, T.; Hasan, H.G. The influence of the inner steel tube on the compression behaviour of the concrete filled double skin steel tube (CFDST) columns. *Mar. Struct.* **2019**, *66*, 197–212. [[CrossRef](#)]
19. Chen, Z.; Xu, R.; Ning, F.; Liang, Y. Compression behaviour and bearing capacity calculation of concrete filled double skin square steel columns. *J. Build. Eng.* **2021**, *42*, 103022. [[CrossRef](#)]
20. Ci, J.; Ahmed, M.; Tran, V.L.; Jia, H.; Chen, S. Axial compressive behavior of circular concrete-filled double steel tubular short columns. *Adv. Struct. Eng.* **2022**, *25*, 259–276. [[CrossRef](#)]
21. Abadel, A.A.; Khan, M.I.; Masmoudi, R. Experimental and numerical study of compressive behavior of axially loaded circular ultra-high-performance concrete-filled tube columns. *Case Stud. Constr. Mater.* **2022**, *17*, e01376. [[CrossRef](#)]
22. Li, J.; Deng, Z. Axial compressive behavior of ultra-high performance concrete-filled double skin high-strength steel tubular short columns. *Struct. Concr.* **2023**, *24*, 3857–3876. [[CrossRef](#)]
23. Yilmaz, B.C.C.; Binbir, E.; Guzelbulut, C.; Yildirim, H.; Celik, O.C. Circular concrete-filled double skin steel tubes under concentric compression: Tests and FEA parametric study. *Compos. Struct.* **2023**, *309*, 116765. [[CrossRef](#)]
24. Hassanein, M.F.; Kharooob, O.F.; Liang, Q.Q. Circular concrete-filled double skin tubular short columns with external stainless steel tubes under axial compression. *Thin-Walled Struct.* **2013**, *73*, 252–263. [[CrossRef](#)]
25. Li, Y.L.; Zhao, X.L.; Raman, R.S.; Yu, X. Axial compression tests on seawater and sea sand concrete-filled double-skin stainless steel circular tubes. *Eng. Struct.* **2018**, *176*, 426–438. [[CrossRef](#)]
26. Wang, F.; Young, B.; Gardner, L. Compressive testing and numerical modelling of concrete-filled double skin CHS with austenitic stainless steel outer tubes. *Thin-Walled Struct.* **2019**, *141*, 345–359. [[CrossRef](#)]
27. Le, T.T.; Patel, V.I.; Liang, Q.Q.; Huynh, P. Numerical modeling of rectangular concrete-filled double-skin steel tubular columns with outer stainless-steel skin. *J. Constr. Steel Res.* **2021**, *179*, 106504. [[CrossRef](#)]
28. Le, T.T.; Patel, V.I.; Liang, Q.Q.; Huynh, P. Axisymmetric simulation of circular concrete-filled double-skin steel tubular short columns incorporating outer stainless-steel tube. *Eng. Struct.* **2021**, *227*, 111416. [[CrossRef](#)]
29. Castanheira, D.S.; De Lima, L.R.O.; Vellasco, P.D.S.; Cashell, K.A.; Gardner, L. Compressive behaviour of double skin sections with stainless steel outer tubes and recycled aggregate concrete. *Structures* **2022**, *41*, 750–763. [[CrossRef](#)]
30. Le, T.T.; Patel, V.I.; Liang, Q.Q.; Huynh, P. Simulation modeling and design of circular concrete-filled double-skin tubular slender beam-columns with outer stainless-steel tube. *Eng. Struct.* **2023**, *285*, 116014. [[CrossRef](#)]
31. Zhou, F.; Lama, L.; Zhao, K. Design of stainless steel CHS-concrete infill-carbon steel CHS double-skin stub columns. *Eng. Struct.* **2023**, *278*, 115479. [[CrossRef](#)]
32. *EN 1994-1-1*; Eurocode 4, Design of Composite Steel and Concrete Structures, Part 1.1: General Rules and Rules for Buildings. European Committee for Standardization (CEN): Brussels, Belgium, 2004.
33. *AS 5100.6-2004*; Bridge Design Part 6: Steel and Composite Construction. Standards Australia: Sydney, Australia, 2004.
34. *ANSI/AISC 360-16*; Specification for Structural Steel Buildings. American Institute of Steel Construction: Chicago, IL, USA, 2016.
35. *ACI 318-14*; Building Code Requirements for Structural Concrete and Commentary. ACI: Farmington Hills, MI, USA, 2014.
36. *T/CCES 7-2020*; Technical Specification for Concrete-Filled Double Skin Steel Tubular Structures. China Architecture & Building Press: Beijing, China, 2020. (In Chinese)
37. *T/CECS 952-2021*; China Association for Engineering Construction Standardization. Technical Specification for Concrete-Filled Stainless Steel Tubular Structures. China Architecture & Building Press: Beijing, China, 2022. (In Chinese)
38. Wang, J.T.; Liu, X.H.; Sun, Q.; Li, Y.W. Compressive–flexural failure mechanism and bearing capacity calculation of over-ranging tapered CFDST members for support structures of offshore wind turbines. *J. Mar. Sci. Eng.* **2023**, *11*, 1621. [[CrossRef](#)]
39. Wang, J.T.; Liu, X.H.; Sun, Q.; Li, Y.W. Analytical behavior and bearing capacity research on out-of-code tapered CFDST members under pure torsion and compression-torsion combination. *Ocean Eng.* **2023**, *284*, 115324. [[CrossRef](#)]
40. Han, L.H. *Concrete Filled Steel Tubular Structures—Theory and Practice*; Science Press: Beijing, China, 2016. (In Chinese)
41. Patel, V.I.; Hassanein, M.F.; Thai, H.T.; Al Abadi, H.; Paton-Cole, V. Behaviour of axially loaded circular concrete-filled bimetallic stainless-carbon steel tubular short columns. *Eng. Struct.* **2017**, *147*, 583–597. [[CrossRef](#)]
42. Tang, G.Q.; Xiao, Y.; Zhang, Y.T. Study of bearing capacity and complete stress-strain curves for concrete filled square steel tube columns. *Eng. Mech.* **2015**, *32*, 103–111. (In Chinese)

Disclaimer/Publisher’s Note: The statements, opinions and data contained in all publications are solely those of the individual author(s) and contributor(s) and not of MDPI and/or the editor(s). MDPI and/or the editor(s) disclaim responsibility for any injury to people or property resulting from any ideas, methods, instructions or products referred to in the content.